Variational Analysis of the Dielectric Rib Waveguide Using the Concept of "Transition Function" and Including Edge Singularities

T. Rozzi, *Fellow, IEEE*, Graziano Cerri, M. N. Husain, and Leonardo Zappelli

Abstract—**Dielectric rib waveguide, being a key transmission medium in millimetrics and integrated optics, has been the object of extensive investigation. Although various approximate analyses of the EDC type exist, these break down for many practical configurations. More complete transverse resonance formulations also exist, but if accuracy is required, they involve mode matching, with a partially discrete, partially continuous spectrum. Whereas finite difference (finite element) numerical solutions are accurate, they are also expensive and their extension to more complex structures is correspondingly difficult.**

In this contribution, we focus on the pure LSE/LSM cases. We derive a highly accurate transverse resonance diffraction variational solution of the problem, of order 1 (a scalar dispersion equation), by assuming at the transverse step discontinuity a single function "trial field" which incorporates the physical properties of the solution. This is, in fact, the surface wave mode of a slab waveguide of height intermediate between that of the rib and that of the cladding slab, including dielectric edge singularities in the LSM case. The height of the "intermediate guide" is obtained by optimizing the overlapping integral with the slab mode in the rib and in the cladding. This criterion turns out to be equivalent to choosing an intermediate guide whose EDC is the geometric mean of those of the rib and cladding. Numerical results are in excellent agreement with those obtained by finite difference, even at cutoff, where the EDC fails and most methods tend to overestimate the value of β.

I. Introduction

RIB waveguide is the most commonly encountered type of waveguide in integrated optics, with likely application to the higher millimetric region. It has, therefore, been the object of much investigation in recent years. Accurate results for the single rib guide have been obtained by purely numerical methods such as finite difference (finite elements) [1]. These are very expensive in computer time, however, and extension to more complicated structures seems correspondingly difficult. Approximate and quasi-analytical methods have also been employed.

For some years, the effective dielectric constant (EDC) in various forms has been the accepted approximation method for the study of waveguides in millimetric and integrated optics [2], [3]. In spite of its simplicity and ease of implementation, its limits are now well appreciated. In 1981 transverse resonance and network methods were combined in studying dielectric guides [4], [5]. In 1984 the image guide problem was approached by transverse resonance diffraction (TRD) [6]. Since then, transverse resonance has been formulated for the rib guide in approximate form [7] and in more rigorous hybrid form [8] by using mode matching at the transverse step discontinuity ($x = 0$ in Fig. 1). In these approaches, the problem is seen as one of diffraction by a transverse step discontinuity, whereupon transverse resonance is employed to derive the propagation constant.

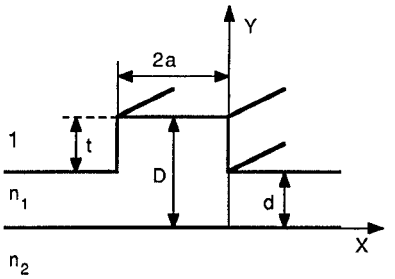

Fig. 1. Geometry of the rib waveguide.

As in a longitudinal step discontinuity problem, direct mode matching does not take into account the true diffraction field at the step and suffers from well-known drawbacks, particularly when a continuum is involved. This problem is not too serious in the LSE case, where the field is regular at the transverse step discontinuity. Correspondingly, all rigorous methods tend to yield more or less accurate values of the propagation constant. It is, however, more serious in the LSM case. For both polarizations, 90° and 270° dielectric corners are at the root of the nonseparability of the problem. In the LSM case in particular, they have an important effect on the field distribution at the plane of the transverse step (see Fig. 4). This aspect has received little attention but is, however, the key to an efficient solution.

In this contribution we shall derive a TRD solution of the rib in the pure LSE/LSM polarizations. It is recognized that the corners above cause the field to be essentially hybrid.

Manuscript received November 17, 1989; revised August 14, 1990.

T. Rozzi is with the Dipartimento di Elettronica e Automatica, University of Ancona, Ancona, Italy, and the School of Electrical Engineering, University of Bath, Bath BA2 7AY, United Kingdom.

G. Cerri and L. Zappelli are with the Dipartimento di Elettronica e Automatica, University of Ancona, Ancona, Italy.

M. N. Husain is with the School of Electrical Engineering, University of Bath, Bath BA2 7AY, United Kingdom.

IEEE Log Number 9041076.

However, for typical aspect ratios and low refractive index differences, the hybrid content is minor, while the effect of nonseparability (and singularity) of the field is a more dominant feature. Moreover, restricting attention to the case of pure polarization introduces a great simplification in the analysis. This simplification is easily removed where required.

In solving the TRD problem, we will adopt a variational formulation of the Rayleigh–Ritz type, i.e., one where we adopt a single function trial field at the transverse step discontinuity, including all known physical features of the discontinuity. The choice of a single function trial field is critical. For instance, using just the surface mode to the right or left of the step is inaccurate because of its *orthogonality* to the continuum.

A very convenient choice turns out to be the modal distribution of a slab of height intermediate between those of the rib and of the cladding layer, which we define as a transition function. In the LSM case we include explicitly the proper singularity of the E field at the corners. As a consequence of the above prudent choice, it is possible to recover a scalar dispersion equation yielding results for the propagation constants and discontinuity fields which are at least as accurate as those obtained by purely numerical methods, but with a fraction of the required computer power/time. It is also noted that the simple two-port transverse equivalent network deriving from a single function trial field is a useful feature with a view to extensions to more complex structures.

II. Even (to x) LSE Analysis

The analysis starts from a knowledge of the complete spectrum of an asymmetric slab waveguide in the y direction, which includes the following.

1) Surface waves, of orthonormalized distribution $\varphi_s(y)$.
2) Air modes, of distribution $\varphi(y,\rho)$, where ρ is a continuous wave number $0 \leqslant \rho < \infty$. Both so-called even and odd waves must be included in view of the lack of symmetry of the problem in the y direction. Where necessary, these will be distinguished by the notation φ_μ: μ = even, odd.
3) Substrate waves, $\varphi_{sb}(y,\sigma)$, $0 \leqslant \sigma \leqslant v = (\epsilon_2 - 1)^{1/2} k_0$.

The spectral expression of the y-directed Hertzian potential $\pi_h(x,y)$ at each side of the step comprises all the above contributions.

E_z and H_y constitute a pair of transverse fields at the discontinuous interface $x = 0$. At each side of the step, these are derived from the potential as

$$E_z(x,y) = j\omega\mu_0 \partial_x \pi_h(x,y) \qquad H_y = \left(\epsilon_r k_0^2 + \partial_y^2\right)\pi_h(x,y). \tag{1}$$

Upon use of spectral expression of the potential in (1), it is possible to obtain an integral relationship of the type

$$E_z(0,y) = \tilde{Z}_L \cdot H_y(0,y) \tag{2}$$

where the kernel $Z_L(y,y')$ of the integral operator $\tilde{Z}_L$ is given by the impedance Green's function:

$$Z_L(y,y') = \frac{1}{j\omega\epsilon_0}\left[-\frac{q_s \tan q_s a}{\epsilon_e}\varphi_s(y)\varphi_s(y') + \sum_\mu \int_0^\infty d\rho\, \gamma \frac{\tanh \gamma a}{1-\left(\frac{\rho}{k_0}\right)^2}\varphi_\mu(y,\rho)\varphi_\mu(y',\rho) + \fint_0^v d\sigma \frac{\eta \tanh \eta a}{\epsilon_2 - \left(\frac{\sigma}{k_0}\right)^2}\varphi_{sb}(y,\sigma)\varphi_{sb}(y',\sigma)\right] \tag{3}$$

where $\fint$ denotes principal value. The wavenumber for bound mode in x is given by

$$k_0^2 - \beta^2 - \rho^2 = -\gamma^2 \qquad \epsilon_2 k_0^2 - \beta^2 - \sigma^2 = -\eta^2$$
$$q_s^2 + \beta^2 = \epsilon_e k_0^2.$$

In (3), we have implicitly assumed that just one surface wave (in y), $\varphi_s(y)$, may be supported by the slab waveguide left of the step. A relationship analogous to (2) exists at the right-hand side of the step, namely,

$$-E_z(0,y) = \tilde{Z}_R \cdot H_y(0,y) \tag{4}$$

where the Green's impedance $Z_R(y,y')$ has a form analogous to (3), after due modification for the semi-infinite region, namely,

$$Z_R(y,y') = \frac{1}{j\omega\epsilon_0}\left[\frac{\gamma_s'}{\epsilon_e'}\psi_s(y)\psi_s(y') + \sum_\mu \fint_0^\infty d\rho \frac{\gamma}{1-\left(\frac{\rho}{k_0}\right)^2}\psi_\mu(y,\rho)\psi_\mu(y'\rho) + \int_0^v d\sigma \frac{\eta}{\epsilon_2 - \left(\frac{\sigma}{k_0}\right)^2}\psi_{sb}(y,\sigma)\psi_{sb}(y',\sigma)\right] \tag{5}$$

where $q_s' = -j\gamma_s'$ corresponds to q_s, ϵ_e' to ϵ_e, and ψ to φ in the region $x \geqslant 0$. With reference to Fig. 1, it is noted that $\psi(y)$ has the same form as $\varphi(y)$, where the appropriate wavenumbers and "d" instead of "D" are used.

The continuity of the fields has been built into (2) and (4). By adding them, we obtain the dispersion equation of the waveguide in the form of an integral equation:

$$\tilde{Z} \cdot H_y(0,y) = 0 \tag{6}$$

where $\tilde{Z} = \tilde{Z}_L + \tilde{Z}_R$.

"Variational" Solution

In the course of a variational development, when choosing expanding functions for the unknown field $H(y) = H_y(0,y)$, it is very advantageous to be able to capture most of the solution with just one term, i.e., a first-order solution. The discussion of the above section seems to suggest that a

prudent choice for H may consist in taking the surface wave, u_s, of a slab waveguide with core height $\bar{d}$ intermediate between d and D ("transition function").

For small steps, there would be little difference between the spectra of the three guides; for larger steps, it seems intuitively reasonable that an intermediate waveguide with EDC $\bar{\epsilon}_e \approx \sqrt{\epsilon_e \epsilon_e'}$ may provide a suitable "transition" between the two waveguides.

More precisely, the transition function u_s overlaps the spectra of both slabs. We seek to optimize the overlap with φ_s and ψ_s, where the latter exists, as the surface waves carry most of the power. Consequently, we choose $\bar{d}$ so as to minimize the error function:

$$\epsilon(\bar{d}) = 2 - (P_s^2 + P_s'^2) > 0.$$

As it turns out, $\bar{d}$ resulting from this condition is but little different from that corresponding to $\bar{\epsilon}_e \approx \sqrt{\epsilon_e \epsilon_e'}$.

It is noted that for d/D sufficiently small, no guidance is present in the cladding slab and the above criterion breaks down. From this point onward we extrapolate for $\bar{d}$ as a function of d.

The evaluation of the overlapping integrals P and P' between u_s and the spectra to either side of the step is facilitated by the following result, which is a particular case of a much more general theorem for calculating the overlapping of two solutions of the wave equation. In particular, we have

$$P_s = \int_{-\infty}^{+\infty} u_s \varphi_s \, dy = \frac{\epsilon_r - 1}{\bar{\epsilon}_e - \epsilon_e} \int_{-\bar{d}}^{0} u_s \varphi_s \, dy$$

$$P_s' = \int_{-\infty}^{+\infty} u_s \psi_s \, dy = \frac{\epsilon_r - 1}{\epsilon_e' - \bar{\epsilon}_e} \int_{-d}^{-\bar{d}} u_s \psi_s \, dy$$

and similarly for the remaining overlapping integrals $P(\rho)$ and $P_{sb}(\sigma)$ with air and substrate modes respectively.

Let us assume the solution $H(y)$ of (6) to be known and multiply this equation on the left by $H(y)$, integrate over y, and divide across by

$$\langle \varphi_s, H \rangle^2 = \left[\int_{-\infty}^{+\infty} \varphi_s(y) H(y) \, dy \right]^2.$$

Isolate then from Z_L, as given in (3), and from Z_R, given in (5), the contributions of the surface waves at each side. The following *scalar* dispersion equation then results:

$$\frac{q_s}{\epsilon_e} \tan q_s a = z_a + z_{sb} + n^2 \frac{\gamma_s'}{\epsilon_e'} \tag{7}$$

where

$$z_a = \sum_{\mu = e,0} \int_0^{\infty} \frac{d\rho}{1 - \left(\frac{\rho}{k_0}\right)^2} \left[\gamma \tanh(\gamma a) P_\mu^2(\rho) + \gamma P_\mu'^2(\rho) \right]$$

$$z_{sb} = \frac{1}{\epsilon_2} \int_0^{v} \frac{d\sigma}{1 - \left(\frac{\sigma}{\epsilon_2 k_0}\right)^2} \left[\eta \tanh(\eta a) P_{sb}^2(\sigma) + \eta P_{sb}'^2(\sigma) \right]. \tag{8}$$

Its transverse equivalent network interpretation is illustrated in Fig. 2. In (8) and in this figure one recognizes four contributions (all within a common factor $1/j\omega\epsilon_0$):

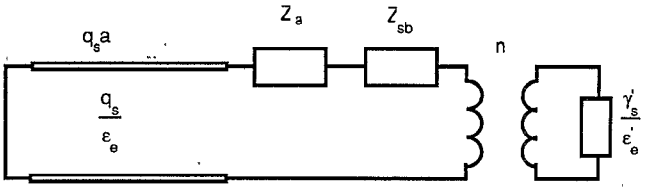

Fig. 2. Equivalent network for the LSE case.

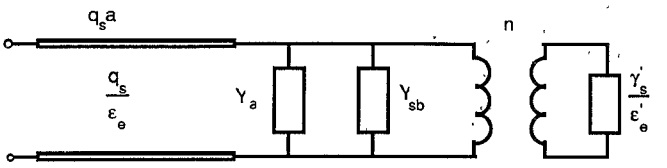

Fig. 3. Equivalent network for the LSM case.

TABLE I
TYPICAL VALUES OF THE ORDER OF THE SINGULARITY NEAR A DIELECTRIC WEDGE OF APERTURE $\theta = \pi/2, 3\pi/2$

ϵ_1	$\alpha = \frac{2}{\pi} \cos^{-1}\left(\frac{1}{2}\frac{\epsilon_1 - 1}{\epsilon_1 + 1}\right) - 1$
1	0
2	−0.107
3	−0.161
5	−0.216
10	−0.268
11.8336	−0.277
20	−0.299
100	−0.326

i) The impedance of the surface wave under the rib, represented by a short-circuited transmission line of electrical length $q_s a$ and characteristic impedance q_s/ϵ_e.

ii) The impedance of the air modes at both sides of the junction as seen by the above surface wave, given by z_a.

iii) The contribution of the substrate modes at both sides of the junction as seen by the surface wave under the rib, given by z_{sb}.

iv) The contribution of the surface wave mode (if any), to the right of the junction, i.e. a load of impedance $1/j\omega\epsilon_0 \, \gamma_s'/\epsilon_e'$ with real γ_s' for a bound mode in the x direction. This load is seen by the surface wave mode under the rib through an ideal transformer:

$$n = \frac{P_s'}{P_s}. \tag{9}$$

The representation given by (7) is quantitatively exact and enjoys variational properties. Although its accuracy depends on an actual knowledge of H, it is noted that H, being transverse to the dielectric wedge along the z axis, is nonsingular [9]. Hence, any reasonable assumption will lead to relatively good results.

If, at this point, the small-step approximation is made:

$$\varphi_s \approx \psi_s \approx H$$

then, by orthogonality, the contributions of air and substrate modes vanish; i.e., $z_a = z_{sb} = 0$ and $n \equiv 1$ in (7) and we are reduced to the EDC calculation.

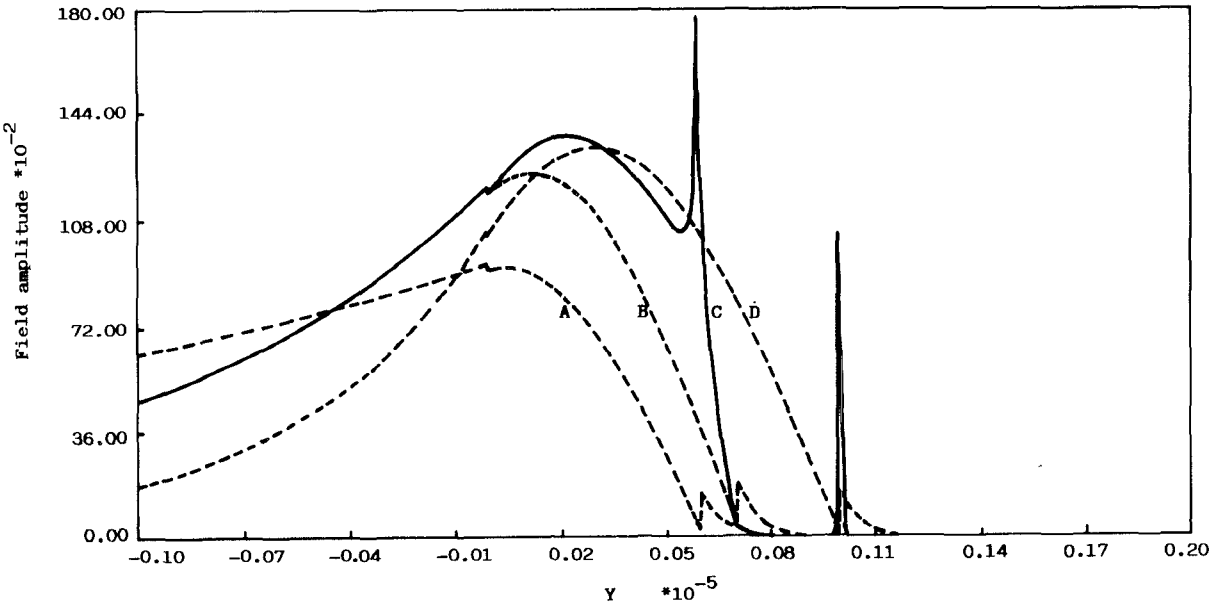

Fig. 4. E_y component of the fundamental LSM mode for slab of heights d (curve A), d (curve B), and D (curve D) compared with the trial field of the transition function (curve C).

It is worth remarking that even when the step is not small, so that φ_s and ψ_s may differ from each other and from H, P_s and P_s' of (9) are both less than unity and their ratio is still fairly close to unity. This fact explains the remarkable accuracy of the EDC calculation in the LSE case not too close to cutoff, where the continuous spectra can no longer be overlooked. The above observation is at the basis of a very accurate first-order variational solution of the step problem.

III. Even LSM Modes

The even LSM modes (TM to y) of the rib waveguide are obtained by placing a magnetic wall on the plane of symmetry $x = -a$, by means of the Hertzian electric potential $\pi_e(x,y)$. The pair of fields, transverse to x, to be used in the analysis are E_y and H_z and these are derived from the potential as

$$E_y = \left(\epsilon_r k_0^2 + \partial_y^2\right)\pi_e(x,y) \qquad H_z = j\omega\epsilon\partial_x\pi_e(x,y). \tag{10}$$

By a development analogous to that of Section II, we arrive at the integral equation for the unknown E_y field at the interface $x = 0$:

$$\tilde{Y}\cdot E_y(0,y) = 0 \tag{11}$$

where

$$Y(y,y') = \frac{1}{j\omega\mu_0}\left[-\frac{q_s\tan q_s a}{\epsilon_e}\varphi_s(y)\varphi_s(y') + \frac{\gamma' s}{\epsilon_e'}\psi_s(y)\psi_s(y') + Y_a(y,y') + Y_{sb}(y,y')\right] \tag{12}$$

and

$$y_a(y,y') = \int_0^\infty d\rho \frac{\gamma}{1-\left(\frac{\rho}{k_0}\right)^2}\left[\tanh(\gamma a)\varphi(y,\rho)\varphi(y',\rho) + \psi(y,\rho)\psi(y',\rho)\right] \tag{13a}$$

$$y_{sb}(y,y') = \frac{1}{\epsilon_2}\int_0^\upsilon d\sigma \frac{\eta}{1-\left(\frac{\sigma}{\epsilon_2 k_0}\right)^2}\cdot\left[\tanh(\eta a)\varphi_{sb}(y,\rho)\varphi_{sb}(y',\rho) + \psi_{sb}(y,\sigma)\psi_{sb}(y',\sigma)\right]. \tag{13b}$$

Again, by a development similar to that of Section II, one deduces the *scalar* dispersion equation

$$\frac{q_s}{\epsilon_e}\tan q_s a = \frac{n^2}{\epsilon_e'}\gamma_s' + y_a + y_{sb} \tag{14}$$

corresponding to the transverse equivalent circuits of Fig. 3, which is the dual of Fig. 2. In the above equation (14), y_a, y_{sb}, and n^2 are defined analogously to (8) and (9), respectively, in terms now of the unknown transverse electric field at the interface $E_y(0,y) \equiv E(y)$ and of the wavenumbers appropriate to the TM case. It is noted, however, that in contrast to the LSE case, E transverse to a dielectric wedge is singular [9]. Hence, $y = d$ and $y = D$ are singular points, as further discussed in the following section, and an appropriate choice of E has more bearing on the accuracy of solution.

The second feature of (14) is, in fact, its close resemblance to (7), which is a dispersion equation for a TM line in x. According to the standard EDC procedure, however, the transmission line representing propagation in the x direction

TABLE II
PARAMETERS OF THE SEMICONDUCTOR RIB WAVEGUIDE STRUCTURES WHICH HAVE BEEN ANALYZED

Rib Guide Structure	n_1	n_2	n_3	D (μm)	d (μm)	$2a$ (μm)	λ (μm)
1	3.44	3.35	1.0	1	varying	3	1.15
2	3.44	3.40	1.0	1	varying	3	1.15
3	3.44	3.34	1.0	1.3	0.2	2	1.55
4	3.44	3.36	1.0	1	0.9	3	1.55
5	3.44	3.435	1.0	6	3.5	4	1.55
6	3.4406	3.4145	1.0	1.5	varying	3	1.15

TABLE III
COMPARISON OF MODE INDICES FOR STRUCTURE 1

d	EDC	TRD Without Continuum	TRD with Continuum		Finite Element [12]
μm	β/k_0	β/k_0	β/k_0	$V=\frac{(\beta/k_0)^2-n_2^2}{n_1^2-n_2^2}$	β/k_0
0.1	—	—	3.406332986899	0.62282131	3.40693
0.2	—	—	3.406453177728	0.62416126	3.40708
0.3	—	—	3.406715746213	0.62708867	3.40725
0.32	3.407806396	3.40642431			
0.4	3.407890320	3.40773878	3.406976578049	0.62999694	3.40746
0.5	3.408093452	3.40807870	3.407276081276	0.63333667	3.40770
0.6	3.408359528	3.40835496	3.407684950229	0.63789640	3.40808
0.7	3.408695221	3.40869350	3.408164053097	0.64324008	3.40856
0.8	3.409144402	3.40914510	3.408818491485	0.65054058	3.40914
0.9	3.409839630	3.40984019	3.409724754287	0.66065259	2.40979

for an LSM mode ought to be of the pure TE type. This apparent incongruity is explained by noting that in the EDC approximation one uses a separable potential of the type $f(y)e^{-jk_x x}$ in each region. Then, one has

$$Y^{\mathrm{TE}}=\frac{H_z}{E_y}=\frac{\omega\epsilon_0\epsilon_r k_x}{\epsilon_r k_0^2-k_y^2}=\frac{\epsilon_r k_x}{\epsilon_e\omega\mu_0}.$$

Only if $k_y\approx 0$ or the identification $\epsilon_r(y)\approx\epsilon_e$ can be made is the characteristic admittance of a TE wave recovered from the above equation. It is, therefore, fair to say that while in the LSE case the EDC is the most basic level of approximation to the rigorous dispersion equation as obtained from transverse resonance diffraction, in the LSM case stronger approximations are required. It is consequently to be expected that the EDC approximation in the LSM case will be further removed from the accurate solution than in the LSE case.

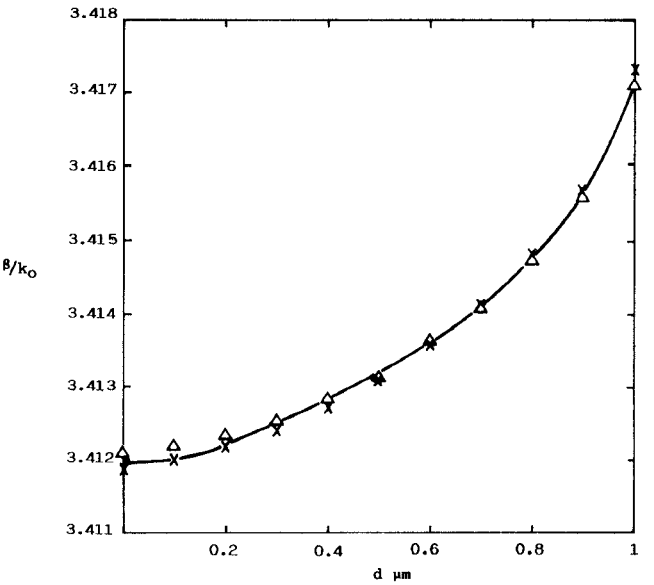

Fig. 5. Normalized propagation constant for the fundamental LSE mode as a function of cladding height. $n_1=3.44$; $n_2=3.40$; $n_3=1.0$; $\lambda=1.15$ μm; $2a=3$ μm; —present analysis; Δ VFEM analysis (ref [1]) *X* SVFDM analysis (ref. [13]).

Edge Singularities: First-Order Variational Solution for E_y

We shall now rigorously solve integral equation (11) by means of a first-order variational approach, taking into account the proper singularities of the transverse electric field at the dielectric corners $y=D$ and $y=d$ of Fig. 1. It is well known [9] that the transverse fields at a dielectric wedge of aperture θ between dielectrics ϵ_1 and 1 are singular like r^α, where r is the distance from the wedge and $\alpha(-1<\alpha<0)$ is given by the lowest eigenvalue of the transcendental equation

$$\sin[(\alpha+1)\pi]\pm\frac{\epsilon_1-1}{\epsilon_1+1}\sin[(\alpha+1)(\theta-\pi)].$$

For $\theta=\pi/2$ (corner $y=D$ of Fig. 1) and $\theta=3\pi/2$ ($y=d$) the order of the singularity is the same and is given by

$$\alpha=\frac{2}{\pi}\cos^{-1}\left(\frac{1}{2}\frac{\epsilon_1-1}{\epsilon_1+1}\right)-1.$$

TABLE IV
COMPARISON OF MODE INDICES FOR STRUCTURES 3, 4 AND 5

Rib Guide		EDC Technique	TRD Analysis (Present Analysis)	Finite Element/Difference [14] FD(1)	[14] FD(2)	[13]
Structure 3	β/k_0	3.390322368	3.388690	3.3906177	3.3912917	3.3869266
	v		0.4832477	0.5025	0.5092	0.4655926
Structure 4	β/k_0	3.395478249	3.3953275	3.3951666	3.3954298	3.3954405
	v		0.4386987	0.4367	0.4400	0.4401
Structure 5	β/k_0	3.437327385	3.4368203	3.4368425	3.4368635	3.4368112
	v		0.3638981	0.3683	0.3725	0.3621

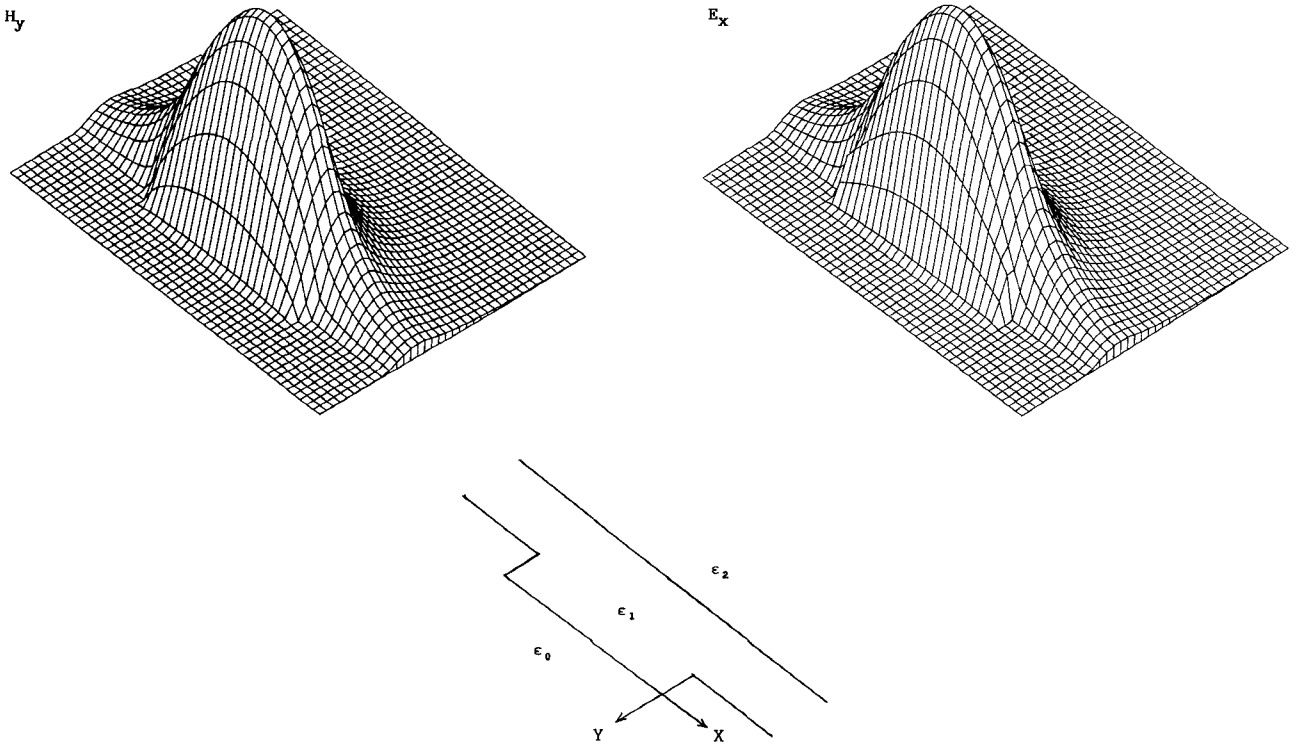

Fig. 6. H_y and E_x field components of the fundamental LSE mode plotted as the magnitude values over transverse guide section.

Typical values of α are reported in Table I. For $\epsilon_1 = 10$, $\alpha = -0.28$, which is a nonnegligible singularity. The typical shape of the true diffraction field at the interface $x = 0$ is the type shown qualitatively in Fig. 4.

Also, a finite jump takes place at the dielectric interface $y = 0$, common to both sides of the step. In order to obtain an accurate variational expression of the lowest possible order, all the above features ought to be built into the trial field.

We used two forms of the trial field involving a transition function where the value of $\bar{d}$ is determined as for the LSE case. The first was of the type of a product of a TM transition function, $\bar{u}_s/\epsilon_r$, times a term describing the singularity, namely

$$E(y) = E_y(0, y) = \frac{\bar{u}_s(y)}{\epsilon_r(y)}\left(1 + \frac{K}{|y-d|^{\alpha}|y-D|^{\alpha}}\right) \quad (15)$$

where K is a variational parameter that minimizes the functional (see (12)):

$$Y = \langle E, \tilde{Y}E \rangle = \frac{1}{j\omega\mu_0}\left[-\frac{qs}{\epsilon_e}\tan(q_s a)P_s^2 + \frac{P_s'^2}{\epsilon_e'}\gamma_s' + y_a + y_{sb}\right]. \quad (16)$$

In view of the relatively complicated nature of (15), the scalar products required in (16), such as

$$P_s \equiv \left\langle \frac{\bar{u}_s}{\epsilon_r}, E \right\rangle$$

need to be evaluated numerically. The above choice (15), however, produces accurate results, which are discussed in the following section.

TABLE V
COMPARISON OF MODAL INDICES FOR THE LSM CASE OF STRUCTURE 2

d μm	Present Analysis With Singularity β/k_0 Using Eq. (15)	Present Analysis With Singularity β/k_0 Using Eq. (17)	Present Analysis Without Singularity β/k_0	Finite Difference Method [13] β/k_0	EDC Technique β/k_0
0.1	3.410202528445	3.4102127	3.410083534325	3.41060	—
0.2	3.410288256175	3.4102402	3.410091441092	3.41073	—
0.3	3.410457938360	3.4102597	3.410119617058	3.41092	—
0.4	3.410678050156	3.4107675	3.410268973640	3.41117	—
0.5	3.410963039520	3.4112158	3.410925733227	3.41150	—
0.6	3.412174130192	3.4118191	3.411380321540	3.41190	3.412707329
0.7	3.412472296772	3.4121408	3.411476035071	3.41241	3.412928581
0.8	3.412978578792	3.4128545	3.412496513103	3.41303	3.413308144
0.9	3.413801442506	3.4135775	3.413784847349	3.41385	3.413937569

TABLE VI
COMPARISON OF MODAL INDICES FOR LSM ANALYSIS OF STRUCTURE 6

d μm	TRD Analysis (Present Analysis) with Singularity β/k_0 Eq. (15)	TRD Analysis (Present Analysis) with Singularity β/k_0 Eq. (17)	TRD Analysis (Present Analysis) Without Singularity β/k_0	EDC β/k_0
0.1	3.423002125351	3.4230844	3.422931208	—
0.2	3.423002226451	3.4231136	3.42293372	—
0.3	3.423003228562	3.4233329	3.42293647	—
0.4	3.423073140853	3.4234474	3.42296027	—
0.5	3.423218060410	3.4235177	3.42304718	—
0.6	3.423488390139	3.4237593	3.42312348	—
0.7	3.423981395150	3.4239557	3.42316368	—
0.8	3.425114321485	3.4243814	3.42318807	3.42567790
0.9	3.425136486940	3.4244065	3.42321265	3.425839424
1.0	3.425393083153	3.4247512	3.42340634	3.426036835
1.1	3.425747334405	3.4252561	3.42390088	3.42627814
1.2	3.426220821181	3.4257251	3.42506294	3.426573753
1.3	3.426766377948	3.426515	3.42646813	3.426946640
1.4	3.427404668557	3.4272225	3.42739956	3.427455902

In order to avoid the above inconvenience also realizing that the effect of each singularity in this problem is well localized to a small neighborhood of the singular corner itself, we used a second trial field, given by

$$
\begin{aligned}
E_y &= \bar{A}e^{-\gamma_0(y-\bar{d})}(y-D)^{\alpha}, \qquad y > D \\
&= \frac{1}{\epsilon_1}\bar{A}e^{-\gamma_0(y-\bar{d})}(D-y)^{\alpha}, \qquad \bar{d} \leqslant y \leqslant D \\
&= \frac{1}{\epsilon_1}\bar{A}\frac{\cos\left(\bar{k}_y y - \bar{\psi}\right)}{\cos\left(\bar{k}_y \bar{d} - \bar{\psi}\right)}(y-d)^{\alpha}\left(\frac{D-\bar{d}}{\bar{d}-d}\right)^{\alpha}, \qquad d \leqslant y \leqslant \bar{d} \\
&= \frac{1}{\epsilon_1}\bar{A}\frac{\cos\left(\bar{k}_y y - \bar{\psi}\right)}{\cos\left(\bar{k}_y \bar{d} - \bar{\psi}\right)}(d-y)^{\alpha}\left(\frac{D-\bar{d}}{\bar{d}-d}\right)^{\alpha}, \qquad 0 \leqslant y \leqslant d \\
&= \frac{1}{\epsilon_2}\bar{A}\frac{\cos\bar{\psi}}{\cos\left(\bar{k}_y \bar{d} - \bar{\psi}\right)}e^{\bar{\gamma}_2 y}d^{\alpha}\left(\frac{D-\bar{d}}{\bar{d}-d}\right)^{\alpha}, \qquad y \leqslant 0 \qquad (17)
\end{aligned}
$$

where

$$\tan\left(\bar{k}_y \bar{d} - \bar{\psi}\right) = \epsilon_1 \frac{\bar{\gamma}_0}{\bar{k}_y}$$

$$\tan\bar{\psi} = \frac{\epsilon_1}{\epsilon_2}\frac{\bar{\gamma}_2}{\bar{k}_y}.$$

We note, in fact, that the above form (17) takes into account each of the two singularities at $y = d, D$ one at a time and includes the dielectric jump at $y = 0$.

Moreover, it is physically clear that no other discontinuity occurs between the two singularities at $y = d, D$. Hence, we assume a continuous function in this interval. For $y > D$, we include the effect of the singularity of $y = D$, whereas the dielectric constant is that of the "air region" above the rib.

The shape of the trial field (17) is compared in Fig. 4 with those of the slab mode in the rib, that of the cladding region, and that of the transition function $\bar{u}s/\epsilon_r$ without inclusion of the singularities for a typical cross section. From the above figure, we note the nonnegligible, but well localized, effects of the two singularities, whereas $\bar{u}s/\epsilon_r$ is seen to have features intermediate between those of φ_s and ψ_s, according to the very concept of transition function.

The advantage of expression (17) with respect to (15) lies in that fact that scalar products such as P_s can be cast analytically (see the Appendix) in terms of incomplete gamma functions. The latter are straightforward to evaluate numerically in rapidly converging series form. For large values of the argument, in fact, the series reduces to a single term. This analyticity of the "scalar products" results in far greater numerical efficiency of the latter trial field, although the actual values of the propagation constants obtained in the two cases are very similar.

IV. NUMERICAL RESULTS

To demonstrate the application of the theory developed in the previous section and the effectiveness of the concept of the transition function, we investigated the propagation

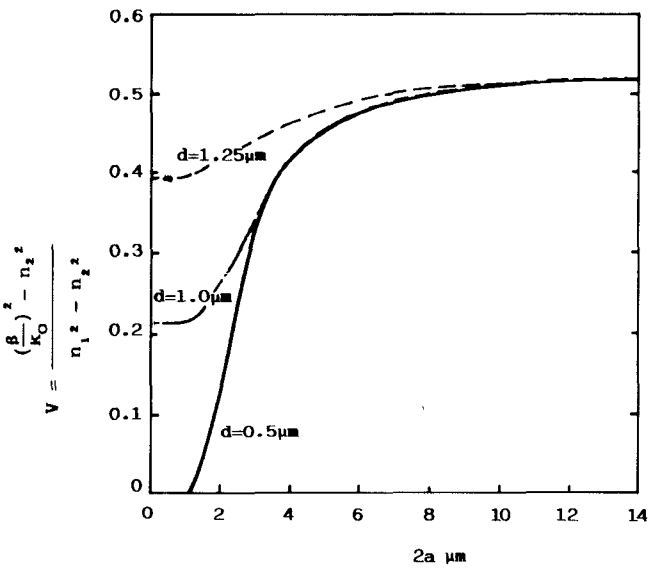

Fig. 7. Normalized propagation characteristics for LSM modes as a function of rib width for three different slab heights. $n_1 = 3.4406$, $n_2 = 3.4145$, $n_3 = 1.0$, $\lambda = 1.15$ μm.

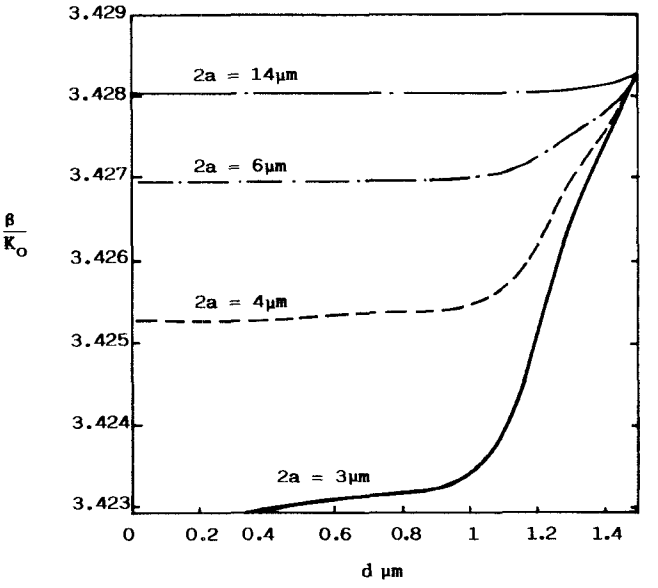

Fig. 8. Normalized propagation constant for the fundamental LSM mode as a function of rib height for different rib widths. $n_1 = 3.4406$, $n_2 = 3.4145$, $n_3 = 1.0$, $\lambda = 1.15$ μm.

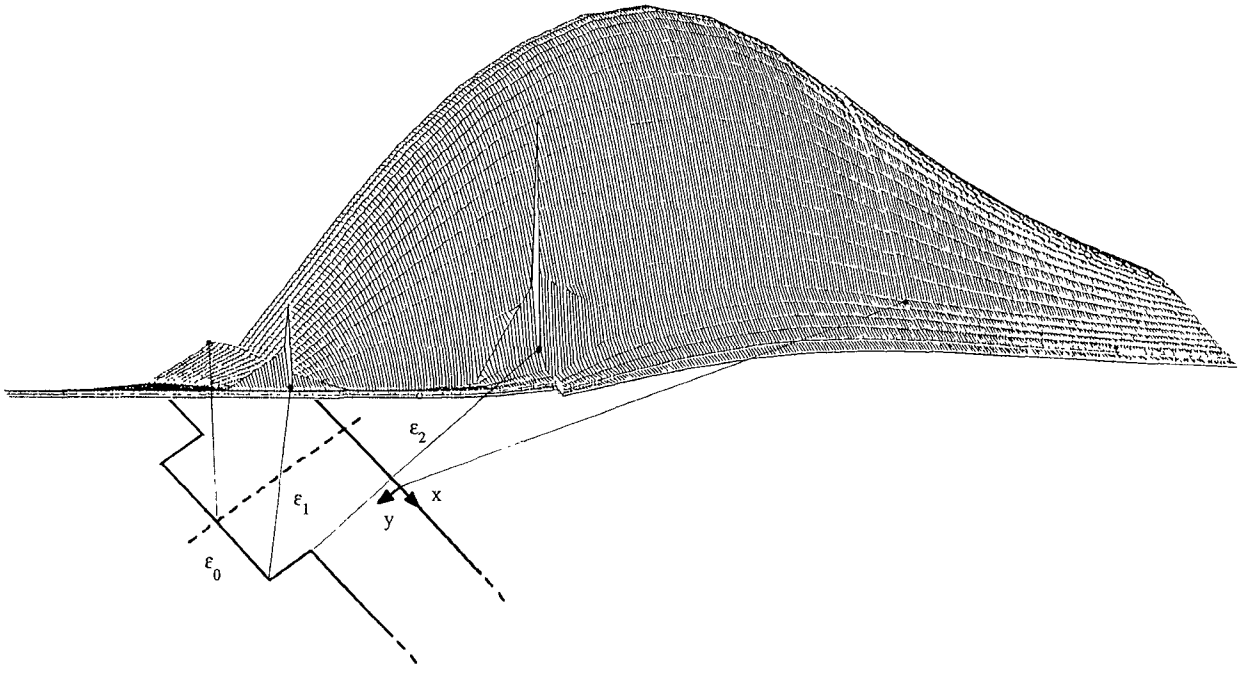

Fig. 9. E_y field components of the fundamental LSM mode plotted as the magnitude values over transverse guide section.

modes of a rib guide whose parameters are illustrated in Table II.

A. LSE Case

In Table III, we report results of modal indices for structure 1 where the thickness of the rib (D) is kept constant while that of the cladding layer d is varied from 0.1 to 0.9. Results obtained by the standard EDC are given in column 2 and compared with those obtained by the above analysis, column 3, but neglecting the effect of the continuum at either side. It is noted that the EDC approximation, as well as that of neglecting the continuum, breaks down for $d \leqslant 0.3$ μm. Column 4 reports present results valid for any value of d. These are compared with column 6, the values obtained in [12] by finite element analysis, for varying values of d.

For a slightly different structure (structure 2), $n_2 = 3.40$, our results are compared with those of the semivectorial FDM analysis [13] and those of vectorial FEM [1] in Fig. 5. Differences, even for large steps, are seen to be minimal. The present results, however, were obtained with a relatively modest computer power effort, typically a minute or two on a mainframe. Had the appropriate library routines been available, even a desktop would have been adequate to the task.

Results on three additional guiding structures (structures 3,4,5), given in Table IV, are found to be in excellent agreement with those of [13] and [14], obtained using the finite element method. Fig. 6 gives a 3-D plot of H_y and E_x. E_x is not directly involved in the solution of the integral equation but is theoretically singular at $x = 0$, $y = D$. Having assumed a nonsingular test function H_y, this feature does not appear. The figure shows, however, the proper discontinuity on the side of the rib at $x = 0$.

B. LSM Case

The LSM case is complicated by the presence of the singularities, as discussed in the previous sections. A comparison between the results obtained using the two trial fields discussed in the previous section for structures 2 and 6 is reported in Tables V and VI respectively. Differences are seen to be minimal, but using the second form is considerably more economical in computer time, as anticipated. Fig. 7 shows the variation of normalized modal indices with rib width for the fundamental LSM mode for three different rib heights. Fig. 8 shows the variation of normalized modal indices for the fundamental LSM mode with rib height for different rib widths. The accuracy of the method is validated by comparing the results with the results of [13] in Table V, where differences are seen to be minimal. Our results in Fig. 7 are also in close agreement with the results presented in [1]. This confirms the assertion made in the introduction that for aspect ratios not too close to unity, the singular behavior near the corner, not the hybrid nature of the field, is the dominant feature of the problem. Finally, a 3-D plot of the E_y field component is provided in Fig. 9, where the presence of the singularity is clearly visible.

V. Conclusions

In this paper, we present a semianalytical treatment of the LSE/LSM polarized rib waveguide based on a variational treatment of the transverse step discontinuity problem of the Rayleigh–Ritz type (a single function trial field) and transverse resonance (transverse resonance diffraction). All known relevant features of the solution are incorporated in the trial field, yielding highly accurate numerical results with modest computer effort. Moreover, a scalar, analytical dispersion equation is recovered which offers some insight and allows extension to more complicated transverse cross sections.

Appendix

In order to give the expressions of $P, P' \cdots$, for the sake of convenience it is necessary to define the following quantities:

$$\Gamma = \left(\frac{D-\bar{d}}{\bar{d}-d}\right)^{\alpha} \qquad \bar{B} = \frac{\bar{A}}{\cos\left(\bar{K}_y \bar{d} - \bar{\psi}\right)}$$

$$\bar{C} = \frac{\bar{A}\cos\bar{\psi}}{\cos\left(\bar{K}y\bar{d} - \bar{\psi}\right)} \qquad B = \frac{A}{\cos\left(hD - \bar{\varphi}\right)}$$

$$C = \frac{A\cos\bar{\varphi}}{\cos\left(hD - \bar{\varphi}\right)} \qquad B_e = \frac{A_e \cos\left(hD - \bar{\varphi}_e\right)}{\cos\alpha_t}$$

$$C_e = A_e \frac{\cos\bar{\varphi}_e}{\cos\alpha_e} \qquad A_s = \sqrt{\epsilon_2} \qquad B_s = \sqrt{\varepsilon_2}\frac{\cos\alpha_{\mathrm{sb}}}{\cos\bar{\varphi}_{\mathrm{sb}}}$$

$$C_s = \sqrt{\epsilon_2}\frac{\cos\alpha_{\mathrm{sb}}}{\cos\bar{\varphi}_{\mathrm{sb}}}\cos\left(hD - \varphi_{\mathrm{sb}}\right).$$

A', B', C', A'_e, B'_e, C'_e, A'_s, B'_s, and C'_s are relative to the slab of height d and are similar to the unprimed values. If the following functions are also defined:

$$\eta = \bar{\varphi} - hd \qquad \xi = \bar{\varphi} - \bar{k}_y d$$

$$\begin{aligned} F_1(\eta,\xi,d,h) = \tfrac{1}{2}\{&\cos(\eta+\xi)\cdot C_\mu\left(d,0,h+\bar{k}_y\right) \\ &-\sin(\eta+\xi)\cdot S_\mu\left(d,0,h+\bar{k}_y\right) \\ &+\cos(\eta-\xi)\cdot C_\mu\left(d,0,h-\bar{k}_y\right) \\ &-\sin(\eta-\xi)\cdot S_\mu\left(d,0,h-\bar{k}_y\right)\} \end{aligned}$$

$$\begin{aligned} F_2(\bar{\varphi},h) = &\cos(\bar{\varphi} - hD)\cdot C_\mu\left(D-\bar{d},-\bar{\gamma}_0,h\right) \\ &-\sin(\bar{\varphi} - hD)\cdot S_\mu\left(D-\bar{d},-\bar{\gamma}_0,h\right) \end{aligned}$$

$$\begin{aligned} F_3\left(\bar{\psi},\bar{k}_y\right) = &\cos\left(\bar{\psi} - \bar{k}_y d\right)\cdot C_\mu\left(\bar{d}-d,p,\bar{k}_y\right) \\ &+\sin\left(\bar{\psi} - \bar{k}_y d\right)\cdot S_\mu\left(\bar{d}-d,p,\bar{k}_y\right) \end{aligned}$$

$$\begin{aligned} F_4(\alpha_t,\rho) = &\cos\left[\alpha_t + \rho(D-d)\right]\cdot C_\mu(d-d,-\gamma_0,p) \\ &+\sin\left[\alpha_t + \rho(D-d)\right]\cdot S_\mu(D-d,-\gamma_0,\rho) \end{aligned}$$

the Fourier coefficients of the field expansion can be written:

$$\begin{aligned} P_s = &\frac{C\cdot\bar{C}\cdot\Gamma d^{\alpha}}{\epsilon_2\cdot(\bar{\gamma}_2+\sigma)} \\ &+\frac{B\cdot\bar{B}\cdot\Gamma}{\epsilon_1}\left[F_1(\eta,\xi,d,h) + F_1(-\eta,-\xi,\bar{d}-d,h)\right] \\ &+e^{-\bar{\gamma}_0(D-\bar{d})}\left[\frac{B}{\epsilon_1}F_2(\bar{\varphi},h) + A\cdot E_\mu(p+\bar{\gamma}_0,0)\right]. \end{aligned}$$

The wavenumber h, p, σ and the phase shift $\bar{\varphi}$ are referred to the TM fundamental mode of the slab of height D.

$$\begin{aligned} P_e(\rho) = &\sqrt{\frac{2}{\pi}}\frac{C_e\cdot\bar{C}\cdot\Gamma d^{\alpha}}{\epsilon_2}\frac{(\bar{\gamma}_2\cos\alpha_e - \sigma\sin\alpha_e)}{(\bar{\gamma}_2^2+\sigma^2)} \\ &+\sqrt{\frac{2}{\pi}}\frac{A_e\cdot\bar{B}\cdot\Gamma}{\epsilon_1}\left[F_1(\eta,\xi,d,h)\right. \\ &\left.+F_1(-\eta,-\xi,\bar{d}-d,h)\right] \\ &+\sqrt{\frac{2}{\pi}}e^{-\bar{\gamma}_0(D-\bar{d})}\left\{A_e F_2(\bar{\varphi}_e,h) + B_e\left[\cos\alpha_t\cdot E_\mu(\bar{\gamma}_0,\rho)\right.\right. \\ &\left.\left.-\sin\alpha_t\cdot H_\mu(\bar{\gamma}_0,\rho)\right]\right\}. \end{aligned}$$

The wavenumber h, σ, ρ and the phase shifts α_e, α_t, and $\bar{\varphi}_e$ are referred to the TM even continuous air spectrum of the slab of height D.

$P_0(\rho)$, relative to the TM odd continuous air spectrum, is obtained by replacing $\alpha_e, \bar{\varphi}_e, \alpha_t$ with $\alpha_0 + \pi/2$, $\bar{\varphi}_0 + \pi/2$, $\alpha_t + \pi/2$, respectively.

$$\begin{aligned} P_{\mathrm{sb}}(\sigma) = &\sqrt{\frac{2}{\pi}}\frac{A_s\cdot C\cdot\Gamma d^{\alpha}}{\epsilon_2}\frac{(\bar{\gamma}_2\cdot\cos\alpha_{\mathrm{sb}} - \sigma\sin\alpha_{\mathrm{sb}})}{(\bar{\gamma}_2^2+\sigma^2)} \\ &+\sqrt{\frac{2}{\pi}}\frac{B_s\cdot\bar{B}\cdot\Gamma}{\epsilon_1}\left[F_1(\eta,\xi,d,h)\right. \\ &\left.+F_1(-\eta_1-\xi_1\bar{d}-d,h)\right] \\ &+\sqrt{\frac{2}{\pi}}e^{-\bar{\gamma}_0(D-\bar{d})}\left[\frac{B_s}{\epsilon_1}F_2(\bar{\varphi}_{\mathrm{sb}},h) + C_s\cdot E_\mu(p+\bar{\gamma}_0,0)\right]. \end{aligned}$$

The wavenumber σ, h, p and the phase shifts α_{sb} and $\bar{\varphi}_{sb}$ are referred to the TM continuous substrate spectrum of the slab of height D:

$$P_s' = \frac{C' \cdot \bar{C} \cdot \Gamma d^{\alpha}}{\epsilon_2(\bar{\gamma}_2 + \sigma)} + \frac{\bar{B} \cdot \Gamma}{\epsilon_1}\left[B' \cdot F_1(\eta, \xi, d, h) + A' \cdot F_3(\bar{\psi}, \bar{K}y)\right]$$
$$+ A' \cdot e^{-(\bar{\gamma}_0 + p)D + pd + \bar{\gamma}_0 \bar{d}} \cdot \left[\frac{1}{\epsilon_1} C_{\mu}(D - \bar{d}, -(\bar{\gamma}_0 + p), 0) + E_{\mu}(\gamma_0 + p, 0)\right].$$

The wavenumbers h, p, σ are referred to the TM fundamental mode of the slab of height d:

$$P_e'(\rho) = \sqrt{\frac{2}{\pi}} \frac{C_e' \cdot \bar{C} \cdot \Gamma d^{\alpha}}{\epsilon_2} \frac{(\bar{\gamma}_2 \cdot \cos\alpha_e - \sigma \sin\alpha_e)}{(\bar{\gamma}_2 + \sigma^2)}$$
$$+ \sqrt{\frac{2}{\pi}} \frac{\bar{B} \cdot \Gamma}{\epsilon_1}\left[A_e' \cdot F_1(\eta, \xi, d, h) + B_e' \cdot F_1(\alpha_t, -\xi, \bar{d} - d, \rho)\right]$$
$$+ \sqrt{\frac{2}{\pi}} B_e' e^{-\bar{\gamma}_0(D - \bar{d})}\left\{\frac{1}{\epsilon_1} F_4(\alpha_t, \rho) + \cos\left[\rho(D - d) + \alpha_t\right] \cdot E_{\mu}(\bar{\gamma}_0, \rho) - \sin\left[\rho(D - d) + \alpha_t\right] \cdot H_{\mu}(\bar{\gamma}_0, \rho)\right\}.$$

The wavenumber h, σ, ρ and the phase shifts α_e, α_t, and φ_e are referred to the continuous TM even air spectrum of the slab of the height d.

$P_0'(\rho)$, relative to the TM odd continuous air spectrum, is obtained by replacing $\alpha_e, \bar{\gamma}_e, \alpha_t$ with $\alpha_0 + \pi/2$, $\bar{\varphi}_0 + \pi/2$, $\alpha_t + \pi/2$, respectively:

$$P_{sb}'(\sigma) = \sqrt{\frac{2}{\pi}} \frac{A_2' \cdot \bar{C} \cdot \Gamma d^{\alpha}}{\epsilon_2} \frac{(\bar{\gamma}_2 \cdot \cos\alpha_{sb} - \sigma \sin\alpha_{sb})}{(\bar{\gamma}_2^2 + \sigma^2)}$$
$$+ \sqrt{\frac{2}{\pi}} \frac{\bar{B} \cdot \Gamma}{\epsilon_1}\left[B_s' \cdot F_1(\eta, \xi, d, h) + C_s' F_3(\bar{\psi}, \bar{k}_y)\right]$$
$$+ \sqrt{\frac{2}{\pi}} e^{-(p + \bar{\gamma}_0)D + pd + \bar{\gamma}_0 d} \cdot C_s' \cdot \left[\frac{1}{\epsilon_1} C_{\mu}(D - \bar{d}, -(p + \bar{\gamma}_0), 0) + E_{\mu}(p + \gamma_0, 0)\right].$$

The wavenumber σ, h, p and the phase shift α_{sb} are referred to the TM continuous substrate spectrum of the slab of height d.

The functions $C_{\mu}(u, \beta, \delta)$ and $S_{\mu}(u, \beta, \delta)$ ($\mu = 1 + \alpha$) are combinations of incomplete gamma functions [10, ch. 3.94 and ch. 8.35], which, in series representation, can be written

$$C_{\mu}(u, \beta, \delta) = u^{\mu} \sum_{n=0}^{\infty} \frac{(-1)^n \left(u \cdot \sqrt{\beta^2 + \delta^2}\right)^n}{n!(\mu + n)} \cdot \cos\left(n \cdot \arctan\frac{\delta}{\beta}\right)$$

and, for large values of $u\sqrt{\beta^2 + \delta^2}$, in the asymptotic form

$$C_{\mu}^{as}(u, \beta, \delta) = \Gamma(\mu)(\beta^2 + \delta^2)^{-\mu/2} \cos\left(\mu \arctan\frac{\delta}{\beta}\right) - u^{\mu} e^{-\beta u} \cdot \sum_{m=0}^{M-1} \frac{(-1)^m \Gamma(1 - \mu + m) \cdot \cos\left[(m + 1)\arctan\frac{\delta}{\beta} + \delta u\right]}{\Gamma(1 - \mu)\left(u\sqrt{\beta^2 + \delta^2}\right)^{m+1}}.$$

$S_{\mu}(\mu, \beta, \sigma)$ is obtained from C_{μ} by replacing u^{μ} and $\cos(\cdot)$ with $-u^{\mu}$ and $\sin(\cdot)$, respectively, and $S_{\mu}^{as}(u, \beta, \delta)$ from the corresponding C_{μ}^{as} by replacing $\cos(\cdot)$ with $\sin(\cdot)$. $H_{\mu}(\beta, \delta)$ and $E_{\mu}(\beta, \delta)$ are given by [10, ch. 3.944.5 and 6].

References

[1] B. M. A. Rahman and J. B. Davies, "Vectorial-H finite element solution of GaAs/GaAlAs rib waveguide," *Proc. Inst. Elec. Eng.*, pt. J, vol. 132, pp. 349–353, 1985.

[2] M. R. Knox and P. P. Toulios, "I.C.'s for the mm. through optical frequency range," in *Proc. MRI Symp. Submillimetre Waves* (New York), Mar. 1970.

[3] T. Rozzi, T. Itoh, and L. Grün, "Two-dimensional analysis of the GaAs d.h. stripe geometry laser," *Radio Sci.*, vol. 2, no. 4, pp. 543–549, July–Aug. 1977.

[4] S. T. Peng and A. A. Oliner, "Guidance and leakage properties of a class of open dielectric waveguides: Part I—Mathematical formulation," *IEEE Trans. Microwave Theory Tech.*, vol. MTT-29, pp. 843–855, Sept. 1981.

[5] A. A. Oliner, S. T. Peng, T. I. Hsu, and A. Sanchez, "Guidance and leakage properties of a class of open dielectric waveguides: Part II—New physical effects," *IEEE Trans. Microwave Theory Tech.*, vol. MTT-29, pp. 855–869, Sept. 1981.

[6] J. Kot and T. Rozzi, "Rigorous modelling of single and coupled image and insular waveguide by TRD," in *Proc. European Microwave Conf.* (Liege), Sept. 1984, pp. 424–429.

[7] N. Dagli and C. Fonstad, "Analysis of rib dielectric waveguides," *IEEE J. Quantum Electron.*, vol. QE-21, pp. 315–319, Apr. 1985.

[8] M. Koshiba and M. Suzuki, "Vectorial wave analysis of dielectric waveguides for optical-integrated circuits using equivalent network approach," *J. Lightwave Technol.*, vol. LT-4, pp. 656–664, June 1986.

[9] J. Bach-Andersen and U. V. Solodukhov, "Field behaviour near a dielectric wedge," *IEEE Trans. Antennas Propagat.*, vol. AP-26, pp. 598–602, July 1978.

[10] I. S. Gradshteyn and I. M. Ryzhik, *Table of Integrals, Series and Products*. New York: Academic Press, 1980.

[11] T. Rozzi, "Rigorous analysis of the step discontinuity in a planar dielectric waveguide," *IEEE Trans. Microwave Theory Tech.*, vol. MTT-26, pp. 738–746, Oct. 1978.

[12] T. M. Benson and J. Buus, "Optical guiding in III–V semiconductor rib structures," in *IEE Conf. Publ. 227* (Cardiff, U.K.), Apr. 1983, pp. 17–20.

[13] M. S. Stern, "Semivectorial polarized finite difference method for optical waveguides with arbitrary index profile," *Proc. Inst. Elec. Eng.*, pt. J, vol. 135, no. 1, pp. 56–63, Feb. 1988.

[14] M. J. Robertson, S. Ritchie, and P. Dayan, "Semiconductor waveguides: Analysis of optical propagation in single rib structures and directional couplers," *Proc. Inst. Elec. Eng.*, pt. J, vol. 132, no. 6, Dec. 1985.

T. Rozzi (M'66–SM'74–F'90) obtained the degree of 'Dottore' in physics from the University of Pisa in 1965, and the Ph.D. degree in electronic engineering from Leeds University in 1968. In June 1987 he received the degree of D.Sc from the University of Bath, Bath, U.K.

From 1968 to 1978 he was a Research Scientist at the Philips Research Laboratories, Eindhoven, the Netherlands, having spent one year, 1975, at the Antenna Laboratory, University of Illinois, Urbana. In 1975 he was awarded the Microwave Prize by the IEEE Microwave Theory and Technique Society.

In 1978 he was appointed to the Chair of Electrical Engineering at the University of Liverpool and was subsequently appointed to the Chair of Electronics and Head of the Electronics Group at the University of Bath, in 1981. From 1983 to 1986 he held the additional position of Head of the School of Electrical Engineering at Bath. Since 1988 Dr. Rozzi has been Professor of Antennas in the Department of Electronics and Control, University of Ancona, Italy, while remaining a visiting professor at Bath University.

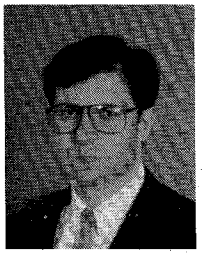

Graziano Cerri was born in Ancona, Italy, in 1956. He received the degree in electronic engineering from the University of Ancona in 1981.

Since 1983, after military service in the Air Force Engineer Corps, he has been with the Department of Electronics and Automatics at the University of Ancona as a researcher. His research deals mainly with microstrip antennas and integrated optics. He is also involved in EMC problems and in the analysis of the interaction between EM fields and biological bodies.

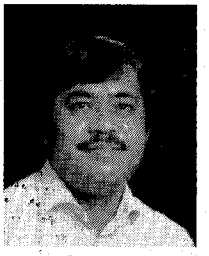

M. N. Husain was born in N. Sembilan, Malaysia, on November 11, 1954. He obtained the Diploma in communication engineering from the Technology University, Malaysia, in 1976, the B.Sc. degree in electrical and electronics engineering from the University of Strathclyde, Scotland, in 1979, and the M.Sc. degree in telecommunication systems from the University of Essex, England, in 1982.

From 1979 to 1981 he was an assistant lecturer on the Faculty of Electrical Engineering, Technology University, Malaysia. In 1982 he was promoted to lecturer at the same university. Since 1987 he has been on leave working toward the Ph.D degree at the University of Bath, Bath, England. His current interests are in the area of millimeter waves and integrated optics, particularly the modeling of waveguide-discontinuity problems.

Leonardo Zappelli was born in Rome in 1962. He received the "Doctor" degree in electronic engineering from the University of Ancona, Italy, in 1987.

Since 1988, he has been with the Department of Electronics and Automatics at the University of Ancona, Italy, as a researcher assistant. His areas of interest are integrated optics and microwaves.